Research Article | Vol. 27, No. 6 | 18 Mar 2019 | OPTICS EXPRESS 8130
Optics EXPRESS

Laser-induced subwavelength structures by microdroplet superlens

EDUARDO CASTILLO-OROZCO,[1,3] RANGANATHAN KUMAR,[1] AND ARAVINDA KAR[2,*]

[1]*Department of Mechanical and Aerospace Engineering, University of Central Florida, Orlando, FL 32816, USA*
[2]*Creol, The College of Optics and Photonics, University of Central Florida, Orlando, FL 32816, USA*
[3]*Escuela Superior Politécnica del Litoral, ESPOL, Facultad en Ingeniería Mecánica y Ciencias de la Producción, Campus Gustavo Galindo, Km. 30.5 Vía Perimetral, P.O. Box 09-01-5863, Guayaquil, Ecuador*
[*]*akar@creol.ucf.edu*

Abstract: Nanoscale patterns on rigid or flexible substrates are of considerable interest in modern nanophotonics and optoelectronics devices. Subwavelength structures are produced in this study by using a laser beam and microdroplets that carry nanoparticles to the deposition substrate. These droplets are generated from an aqueous suspension of nanoparticles by electrospray and dispensed through a conical hollow laser beam so that laser-droplet interactions occur immediately above the substrate surface. Each microdroplet serves the dual role as a nanoparticle carrier to the substrate and as a superlens for focusing the laser beam to a subwavelength diameter. This focused beam vaporizes the droplet and sinters the nanoparticles on the substrate. The deposition of subwavelength nanostructures and thin films on a silicon wafer are demonstrated in this paper. This process may be applied to produce novel nanophotonics and electronics devices involving a variety of subwavelength patterns including an ordered array of semiconductor nanoparticles.

1. Introduction

Delivering nanomaterials to substrates for producing subwavelength structures is of interest in the fabrication of optoelectronic, energy and electronic components such as light-emitting diodes [1], solar cells [2], and sensors, actuators and ultra-flexible electrodes for neuro-stimulators and prosthetics [3]. Also, the fabrication of nanostructures on flexible and stretchable substrates is important for the development of novel electronic and photonic devices. Inorganic compounds such as MXene has been used to produce conducting and flexible thin films. An et al. [4] used layer-by-layer deposition to layer various nanosheets of two-dimensional metal carbides in between polymer sheets. Thomas et al. [5] fabricated densely packed micro and nanoscale polymer features using melt processing. Chemically synthesized semiconductor nanowires have been investigated for applications in electronic and photonic devices. Liu et al. [6] reported the chemical growth of zinc oxide nanorod arrays on a flexible thermoplastic polyurethane substrate by sputtering ZnO seeds. In addition, ZnO nanorods can be electrochemically deposited on flexible conductive substrates such as gold film [7]. Single-walled carbon nanotubes synthesized by chemical vapor deposition [8] using methane as the feed gas and iron as the catalyst can form percolating networks that exhibit semiconducting properties [9] and may be used in flexible optoelectronics. Semiconductor materials have been patterned on flexible substrates using conventional inkjet printing to produce microelectrodes [10,11]. Recently Saleh et al. [12] employed an aerosol jet technology to produce three-dimensional micro-engineered materials, such as micro-lattices, by direct printing of nanoparticle dispersions. Potential applications of micro-lattices include ultralight or multifunctional materials, micro-optoelectronics, microfluidics, and tissue

#354798 https://doi.org/10.1364/OE.27.008130
Journal © 2019 Received 7 Dec 2018; revised 18 Jan 2019; accepted 19 Jan 2019; published 6 Mar 2019

Optics EXPRESS

engineering. The materials printed by conventional techniques such as inkjet or aerosol jet, however, require substantial heat-treatment to vaporize the organic ink material that binds the nanoparticles before and during the printing process.

Compared to the conventional techniques, the femtosecond laser-assisted nanofabrication provides a fast and noncontact process for patterning nanostructures. A few novel methods have been developed to produce these nanostructures. Tseng et al. [13] demonstrated geometric patterns of nanodots and rings [14] of $Ge_2Sb_2Te_5$ using laser-induced forward transfer of materials. Kuznetsov et al. [15] deposited nanodot arrays by laser-induced backward transfer of gold nanodroplets. Also, lithography techniques such as laser interference lithography [16], two-photon polymerization nanolithography [17] and laser microlens array lithography [18] have been utilized to fabricate two- and three-dimensional nanostructures. In the Nano-Electrospray Laser Deposition (NELD) of the present study, an aqueous suspension of nanoparticles, i.e., an aqueous ink, and a laser beam are used and, therefore, the water is evaporated and simultaneously the nanoparticles are sintered by the beam as the deposition occurs.

To produce subwavelength structures, however, subwavelength focusing of the laser beam is necessary so that nanodots and thin films of width smaller than the laser wavelength, or nanodiameter holes in a substrate for ultrafine filtration and photonic crystals can be produced. Wang et al. [19] used a microparticle mask for nanostructuring a substrate surface by irradiating the mask with a pulsed laser. In another study, Wang et al. [20] demonstrated subwavelength focusing by SiO_2 microspheres and provided a mathematical analysis for this superlens effect. Photonic nanostructures [21,22], random nanoparticles [23,24], solid microspheres [25,26], and liquid droplets [27,28] have been utilized to produce subwavelength structures on a variety of substrates. Smolyaninova et al. [27] demonstrated the superresolution properties of deformed microdroplets of glycerin on the surface of gold film when the microdroplets emulated the refractive index distribution of Maxwell fish-eye (MFE) or Eaton lens. Duocastella et al. [28] employed a hemispherical droplet, which was a solution of water and glycerol (50% by volume) with 1% sodium dodecyl sulfate surfactant on a polydimethylsiloxane (PDMS) substrate, as a lens for thin film deposition of subwavelength width $\lambda_0/4$ using a laser of wavelength λ_0 = 1027 nm and a microscope objective where λ_0 is the wavelength in vacuum. These focusing techniques are, however, not readily amenable to continuously produce subwavelength structures since the methods require close proximity between the lens and substrate, and does not provide a convenient means of supplying fresh nanoparticles to the focused laser beam. In the present study, the dual role of microdroplets provides a convenient mechanism to supply nanoparticles to the substrate and simultaneously focus the laser beam for producing subwavelength structures. This mechanism is intended to evolve further for fabricating nanostructures and nanopatterns including applications in plasmonic structures [29–31], resonators [32,33], and metasurfaces [34].

Optics EXPRESS

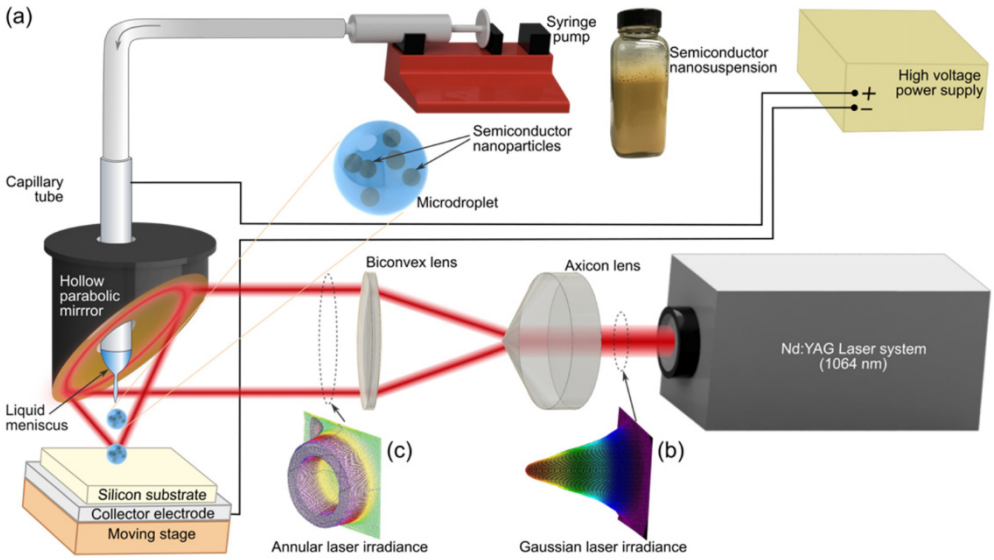

Fig. 1. Microdroplet superlens of dual role for carrying nanoparticles and subwavelength focusing: (a) An experimental setup for dispensing aqueous microdroplets of nanoparticle suspension into a conical hollow laser beam to achieve subwavelength focusing by the microdroplets, (b) Gaussian laser beam produced by the Nd:YAG laser system, and (c) Collimated laser beam of annular irradiance profile.

2. Experimental Procedure

The suspensions used in this study were aqueous colloidal suspensions of silver, silicon, and germanium nanoparticles and a surfactant solution as listed in Table 1. The Ag, Si, and Ge nanoparticles were 99.95% pure with an average particle size 30 nm and standard deviation 20 nm; 99.9% pure with an average particle size 40 nm and standard deviation 20 nm; and 99.99% pure with an average particle size 290 nm and standard deviation 200 nm respectively, with the specific size distribution approximately fitting a log-normal distribution. For Ge nanoparticles there was a small number of large particles that settle down in the liquid, resulting in a nanosuspension of particle size less than or equal to 300 nm. All suspensions were prepared by dispersing the nanoparticles in de-ionized (DI) water and adding dispersant and surfactant to the mixture of the water and nanoparticles. The suspensions were ultrasonicated at 20 kHz for an hour. The surfactant and dispersant were sodium dodecyl sulfate and sodium salt of poly-naphthalene sulfonic acid respectively. The colloidal suspensions were injected into a hollow laser beam using a syringe pump and electric field between the capillary tube and substrate as illustrated in Fig. 1. The electrospray apparatus operates in three modes called dripping, microdripping and oscillating microdripping modes, and the microdripping mode generates microdroplets of nearly the same diameter at a steady rate [35]. The microdripping mode was employed in this study because the operation of the electrospray system is stable in this mode for generating a steady stream of microdroplets. The semiconductor suspensions were used to deposit nanodots on a rigid Si substrate; while the Ag suspension to create conductive line and film on the same rigid Si substrate and on a flexible paper substrate. In addition, the surfactant solution, which did not contain any nanoparticles, i.e., the sample Ge0 in Table 1, was used to create subwavelength holes on a Si substrate.

Table 1. Physical properties and relevant parameters of nanoparticle suspensions in DI water.

Liquid	Density	Viscosity	Electrical conductivity	Surface tension	Droplet radius

Optics EXPRESS

	g/ml	mPa.s	μ S/cm	mN/m	μ m
Ge0*	1.000	1.10	595.0	49.8	38.3
Ge2	1.023	1.36	718.2	47.2	38.1
Ge5	0.064	1.56	797.8	47.5	37.9
Ge10	0.130	1.95	898.4	47.6	37.7
Si5	1.033	1.82	1391.6	48.2	39.8
Ag20	1.153	1.71	1202.0	47.2	150.0

*Numeral suffixes denote wt% of the semiconductor materials Ge and Si and the metallic Ag material.

Si and Ge nanosuspension microdroplets of radius ranging 10 to 70 μm were produced at a steady rate of 420 droplets per second in the microdripping mode by applying 3300 V between the capillary tube and the substrate to investigate subwavelength focusing, as shown in Fig. 1(a). The focusability of microdroplets changes from subwavelength focusing to large diameter focal spot when the droplet size increases. Under this condition, the nanoparticles deposit as a thin film on the substrate. For testing the effect of large diameter focal spots, the radius of microdroplets was increased to a size ranging from 100 to 150 µm and Ag nanoparticles were observed to deposit on a flexible substrate such as a paper cardstock. A pulsed Nd:YAG laser of wavelength λ_0 = 1064 nm was used as the input laser beam, as shown in Fig. 1(b). An axicon lens and a biconvex lens were used to shape the Nd:YAG Gaussian laser beam into an annular beam of nearly uniform radial irradiance distribution, as shown in Fig. 1(c). The microdroplets were injected into the empty space of the annular beam through the hole of a special hollow parabolic mirror. The annular beam was focused by the parabolic mirror to form a hollow laser cone and refocused by the microdroplet during the laser-droplet interactions in the vicinity of the apex of the cone near the substrate surface. To gain insight into the effect of the droplet size on the laser-droplet interaction, the reflectance and absorption coefficient of the samples are presented in Fig. 2. The reflectance data in Fig. 2(a) indicate that a certain fraction of the incident Nd:YAG laser energy will be reflected by the droplet at the wavelength λ_0 = 1064 nm, and the rest of the energy will propagate through the droplet. The absorption coefficient data in Fig. 2(b), on the other hand, provide the depth of penetration by the laser inside the droplet since the penetration depth is the reciprocal of the absorption coefficient. The penetration depths for the samples Ge0, Ge2, Ge5, Ge10, Si5, and Ag20 are 50 mm, 20 mm, 2.4 mm, 1.3 mm, 1.6 mm and 100 µm, respectively, at λ_0 = 1064 nm. Small droplet size and large penetration depth of the Ge and Si samples suggest that much of the laser beam will pass through the droplet to reach the substrate surface and the droplet will evaporate after impinging on the substrate. This condition is suitable for nanoparticle deposition on rigid substrates since much of the laser energy is utilized to heat the substrate which subsequently evaporates the droplet. The droplet size and penetration depth of the Ag sample are comparable, indicating that much of the laser energy will be absorbed by the droplet and a small amount of the energy will reach the substrate. This condition is suitable for nanoparticle deposition on a flexible substrate since much of the laser energy is utilized for internal heating of the droplet and less energy is available for heating the substrate.

Optics EXPRESS

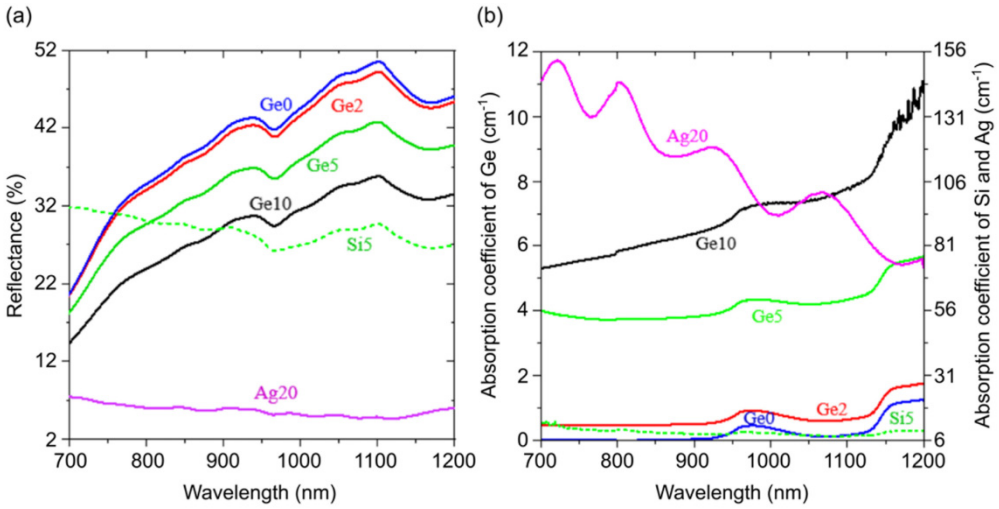

Fig. 2. Optical properties of nanosuspensions. (a) Reflectance data based on 0.012 mm think Ag20 sample and 1 mm thickness for other samples. (b) Absorption coefficient determined by measuring the optical density of the nanosuspensions.

Laser heating of the droplets evaporates the water and sinters the nanoparticles to form microlayers on the substrate when the substrate is moved continuously using an X-Y stage. The speed of the substrate and the droplet size can be varied for depositing thin films, lines and regular arrays of microdots as well as nanodots. The X-Y motorized stage was used to move the silicon substrate continuously at the speed of 0.1 mm/s during the deposition process. The laser system was operated at the pulse repetition rate of 30 kHz and pulse length of 170 ns, and the average powers of the laser were selected as 5, 9, 13, 17 and 22 W. The diameter of the laser beam on the rigid Si surface was 285 μm for deposition of nanodots and formation of subwavelength holes. For the flexible substrate, the laser was defocused to produce a spot of diameter approximately 3 mm and the scanning speed was increased to 1 mm/s to avoid burning the paper cardstock. Similarly, silver films were observed to deposit on the silicon substrate when the radius of the microdroplet was 150 µm and laser spot diameter and scanning speed were 500 μm and 0.1 mm/s, respectively.

High-speed photography (Phantom V12.1 camera) was used for imaging the microdroplet generation, microdroplet heating process, evaporation of the liquid, and subsequent sintering of the nanoparticles. An in-house Matlab code was used to analyze and process the high-speed images. The subwavelength holes and nanostructures were analyzed using optical profilometry (4D Technology NanoCam Sq), SEM microscopy and EDS analysis (Zeiss ULTRA-55 FEG SEM). Ultrasonication at 20 kHz for 10 min was used to clean the silicon substrate before and after the laser deposition experiment. This procedure yields clean samples by removing the excess nanoparticles that are not completely sintered during the NELD process.

3. Results

The interaction of the laser beam with the microdroplets of nanosuspension can be classified into three stages as illustrated in Fig. 3. The laser heating process begins when the microdroplets, which are injected into the hollow laser cone, meet the laser beam on their way to impinge on the substrate, as shown in Fig. 3(a). Each microdroplet initially acts as a lens to cause geometrical focusing of the beam depending on the curvature and refractive index of the droplet. The laser beam, on the other hand, propagates through the droplets and acts as a volumetric heat source for heating the interior of the droplets. The radii of the microdroplets

Optics EXPRESS

vary from 10 to 70 μm with an average radius of 35 to 40 μm depending on the semiconductor nanosuspensions tested in this study. The focal spot diameter achieved in this first stage is diffraction-limited and was estimated to be between 1.8 - 2.5 μm for the cases of this study. In the second stage, interference occurs due to the superposition of the conical hollow laser beam at the apex of the cone, and the resulting irradiance distribution, which is proportional to $J_0^2(kr)$, is similar to a Bessel beam, where k, r, and J_0 are the spatial angular frequency or wavenumber, radial coordinate perpendicular to the direction of laser beam propagation, and first kind Bessel function of order zero, respectively. In addition, the curvature of the microdroplet surface concentrates the electromagnetic field like a lens [36,37] and, therefore, enhances the laser irradiance, as shown in Fig. 3(b). Consequently, the laser irradiance varies inside the droplets in both vertical and horizontal directions due to the interference and focusing effects respectively, resulting in nonuniform heating with significant temperature variation in the droplets. As a consequence, the temperature at the bottom of the microdroplet is increased and this can promote thermo-capillary convection within the droplet to cause heating of the liquid which is not directly heated by the laser beam. The inset in Fig. 3(b) is a photograph of a microdroplet, showing the fringe patterns caused by the interference of the focused annular laser and the enhanced irradiance at the bottom of microdroplet. Finally, in the third stage, the droplets impinge on the substrate and the liquid evaporates to deposit the nanoparticles on the substrate, as shown in Fig. 3(c). The inset in this figure is a photograph of the liquid film on the substrate surface. This picture, which was observed with high-speed photography, shows multiple ripples of small radii of curvature at the surface of the liquid film. The nonuniform heating of the droplet causes nonuniform surface evaporation and, consequently, the original smooth surface of the liquid is deformed into multiple curved surfaces of small radii of curvature. Vapor bubbles can also contribute to the formation of curved surfaces. The bubbles are generally produced due to heterogeneous nucleation at the surface of the suspended nanoparticles and the solid substrate.

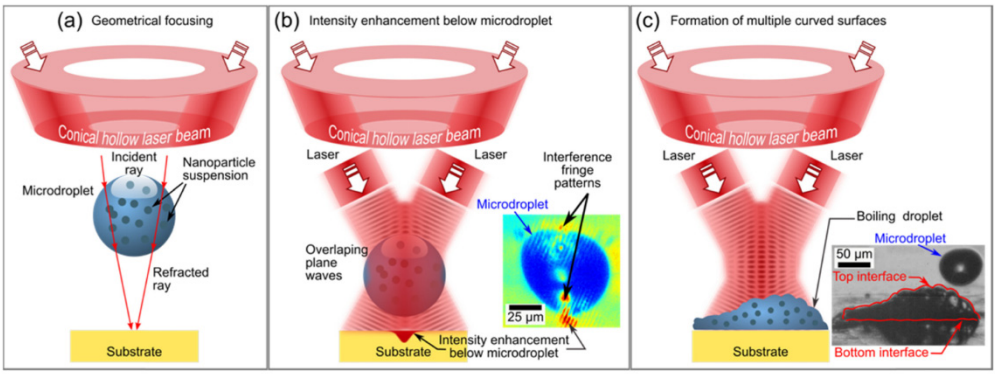

Fig. 3. Laser-droplet interactions for heating the droplets: (a) Geometrical focusing of the laser beam when the microdroplet acts as a lens. (b) Incident laser on top of the microdroplet and intensity enhancement below the same microdroplet. The photographic inset shows the fringe patterns caused by the interference of the annular laser at the focal volume. The intensity enhancement at the bottom of microdroplet is observed by image processing of the droplet photograph. (c) Incident laser on an evaporating droplet after the droplet impinges on the substrate, exhibiting a wavy top surface with ripples of radii much smaller than the radius of the microdroplet so that each curved segment can focus a portion of the laser beam. The composition of droplets depicted in (b) and (c) is Ge, 2 wt% in DI water.

The effect of microdroplets containing semiconductor nanoparticles is presented in Fig. 4, showing the scanning electron microscopic (SEM) images of an array of Ge nanodots on a Si substrate for a suspension of 5 wt% Ge in DI water. Similarly, Fig. 5 shows the SEM images

Optics EXPRESS

of Si nanodots deposited on a Si substrate using a suspension of 5 wt% Si in DI water. The diameters of the nanodots vary from 100 nm to 500 nm, which are smaller than the incident laser wavelength of 1064 nm. The results in these two figures were obtained with an input laser power of 17 W. Although deposition of nanodots is achieved, they exhibit a random pattern that can affect their optical properties. Reasons for this unsystematic patterns are discussed later in section 4. However, a strategy to improve the pattern from a random distribution of nanodots to a regular array could be to use microdroplets of more viscous nanosuspension for preventing the spreading of nanodots during the deposition process, or tinier microdroplets containing fewer nanoclusters.

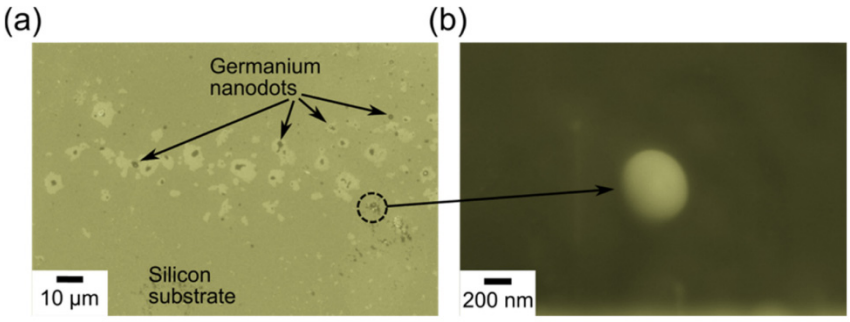

Fig. 4. Germanium nanodots on a silicon substrate: (a) SEM image of a linear array of Ge nanodots produced by microdroplets of Ge suspension, 5 wt% Ge in DI water and incident laser power 17 W, and (b) SEM image at a higher magnification, showing a nanodot of approximately 500 nm diameter.

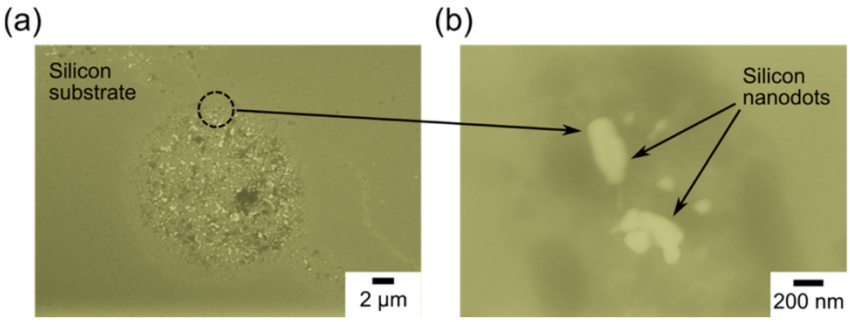

Fig. 5. Silicon nanodots on a silicon substrate: (a) SEM image of Si nanodots (cluster of Si nanoparticles) of diameters ranging from 100 nm to 500 nm that were produced by microdroplets of Si suspension, 5 wt% Si in DI water and an incident laser power 17W, and (b) SEM image at a higher magnification, showing the shapes of the nanodots.

Subwavelength structures were also observed at the substrate surface when the microdroplets were just a surfactant solution in DI water containing no nanoparticles. Figure 6(a) shows SEM images of subwavelength holes of diameters varying from 100 to 200 nm on a Si substrate, indicating the superlens effect of the droplets since the wavelength of the incident laser was 1064 nm. The depth of the holes in Fig. 6(b) is found to be approximately 120 nm. Also, a rim is formed by the resolidification of the Si melt around the entrance of the hole and this rim protrudes approximately 30 nm above the original substrate surface. The results in Figs. 6(a) and 6(b) were obtained with an input laser power of 17 W.

The effect of laser power on the formation of subwavelength features is presented in Fig. 7 for microdroplets containing 0 wt% (i.e., surfactant solution only, no Ge suspension), 2 wt%, 5 wt%, and 10 wt% Ge in DI water. These liquids were supplied to the capillary tube by the syringe pump at a flow rate of 10 μL/min and the microdroplets were generated at a

Optics EXPRESS

frequency of 420 droplets/s, resulting in microdroplets of average radius 35 to 40 μm. Figure 7 indicates that there is a narrow range of laser power for creating subwavelength structures. At low laser powers, the droplets do not vaporize significantly and the nanoparticles do not sinter to adhere to the substrate due to insufficient energy. At high laser powers, on the other hand, the droplets are heated excessively causing a change in their surface tension property and the contact angle between the droplet and substrate. So the droplets bounce off the substrate like water droplets on hot skillets due to a physical phenomenon called Leidenfrost effect [38,39], causing no deposition of nanoparticles on the substrate.

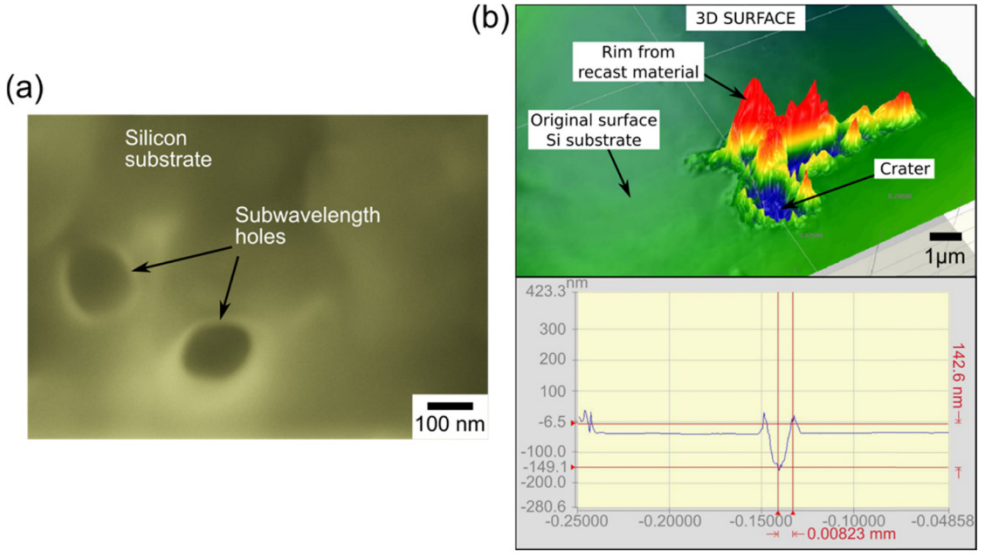

Fig. 6. Subwavelength holes on a silicon substrate: (a) SEM image of subwavelength holes of size ranging from 100 nm to 200 nm produced with a laser of incident power 17 W, and (b) Optical profiles of the holes obtained with a laser interferometer. Three-dimensional surface measurement shows the presence of tiny indentations with the depth of the crater approximately 120 nm and the height of a typical rim formed from the recast silicon approximately 30 nm above the original substrate surface.

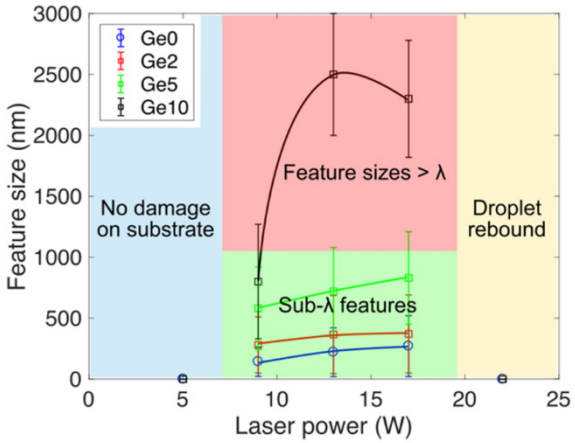

Fig. 7. Feature sizes as a function of the incident laser power for microdroplets of liquids containing 0 wt%, 2 wt%, 5 wt%, and 10 wt% Ge nanoparticles in DI water.

Optics EXPRESS

The focusability of the droplets changes if the diameters of the laser beam and droplets are large. This variability in the optical property of the droplets makes the NELD process versatile since both subwavelength features and thin films can be produced by the same process under different operating conditions. A thin line of Ge is deposited on a silicon substrate as shown by the SEM image in Fig. 8(a). This line is approximately 50 μm wide and was produced by depositing a new layer after the previous one for five times using microdroplets of 10 wt% Ge suspension in DI water at a flow rate of 50 μl/min and an input laser power of 17 W. Figure 8(b) is a compositional analysis of the Ge line by energy-dispersive X-ray spectroscopy (EDS), showing the presence of C, O, Na, Ge and Si, and confirming the deposition of Ge by the NELD process. The presence of C is due to the carbon tape used to attach the sample to the sample holder of the SEM instrument. The presence of O may be due to the surrounding atmosphere since the deposition experiment was performed in an open atmosphere, or due to the native oxide SiO_2 on the Si substrate. The source of Na is traced to the surfactant (sodium dodecyl sulfate) and dispersant (sodium salt of poly-naphthalene sulfonic acid) that were used to keep the Ge nanoparticles suspended in DI water.

Larger thin films can also be deposited on textured flexible substrates such as paper cardstock as shown in Fig. 9(a) or on rigid substrates such as Si in Fig. 9(b). Wider films can be deposited by an appropriate selection of the laser power and beam diameter, and the size and frequency of droplet delivery to the substrate. The silver films in Figs. 9(a) and 9(b) were produced using microdroplets of 20 wt% Ag suspension in DI water. The suspension was delivered by the syringe pump to the capillary tube at a flow rate of 100 μ L/min. Droplets of average diameter 300 μ m were produced by the capillary tube at the frequency of 300 droplets/s for an applied voltage of 2800 V over a distance of 8 mm between the substrate and the tip of the capillary tube. These droplets were irradiated with a laser of incident power 13 W. The laser beam was defocused to produce a spot of approximately 3 mm diameter for depositing Ag film on cardstocks and the spot diameter was 0.5 mm for depositing Ag film on Si wafers. Figure 9(a) shows that a thin Ag film of approximately 2 mm wide, which was deposited on a cardstock, can be bent without any mechanical damage to the film. Figure 9(b), on the other hand, shows the deposition of Ag thin film tracks on a Si wafer with each track separated by a small distance of approximately 15 μm. The inherent advantage of localized heating by the laser enabled this type of deposition without thermally damaging the substrates.

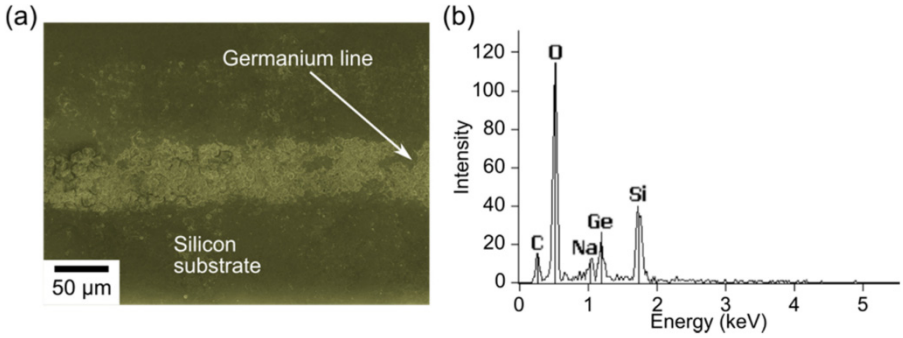

Fig. 8. Deposition of a Ge line on a Si wafer: (a) SEM image of a thin line of Ge deposited by the NELD process on a Si substrate using microdroplets of a suspension of 10 wt% Ge nanoparticles in DI water at the flow rate of 50 μL/min and a laser of incident power 17 W. The 50 μm wide film was constructed by depositing a new layer after the previous one for five times. (b) EDS analysis of the Ge film, showing the presence of Ge in the laser-sintered line.

Optics EXPRESS

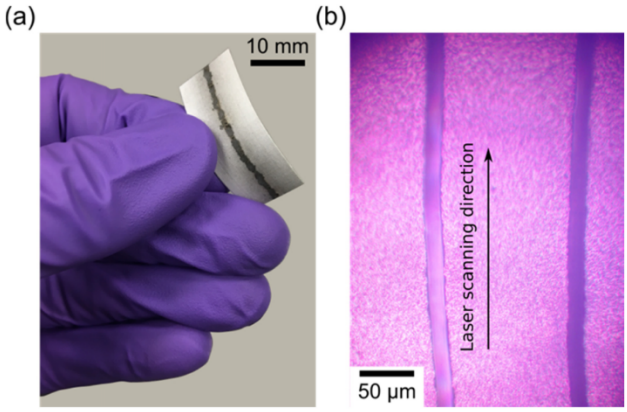

Fig. 9. Deposition of thin films on flexible and rigid substrates: (a) Bending test for a silver thin film of approximately 2 mm wide deposited on a paper cardstock, and (b) Deposition of silver thin film tracks on a smooth silicon wafer.

4. Discussion

As presented in the previous section, the interaction between a laser and microdroplet can cause subwavelength focusing. A microdroplet acts as a lens due to its curvature, which affects the focal length (f) of the lens, and refractive index (n) while it travels through the hollow conical laser beam, as illustrated in Fig. 3(a). The diffraction-limited Gaussian laser beam diameter, D, at the focal spot depends on f and n as $D = \frac{4 f \lambda_0}{\pi n D_L}$, where D_L is the laser beam diameter at the incident surface of the lens. The concentration of nanoparticles increases in the microdroplet during the evaporation of the droplet by the laser beam and, therefore, the value of n can increase, resulting in a smaller focal spot size. However, the laser heating of the microdroplet can also cause spatially varying refractive index distribution that may contribute to subwavelength focusing. Miñano [40] has shown that superresolution property can be achieved in spherical lenses with a variety of distributions of the refractive index, including a spherical core of constant refractive index surrounded by a spherical shell of varying refractive index. These refractive index distributions are different from that of the MFE lens. Miñano et al. [41] have also studied the perfect focusing capability of waveguides formed by spherical shells and pointed out that the shells are expected to behave very close to the MFE lens if they are very thin so that the refractive index has a certain constant value within the shell. These studies suggest that other conditions for the refractive index variation may exist in liquid microdroplets to enable subwavelength focusing.

On the other hand, the curved surfaces and the scattering of laser by the nanoparticles as illustrated in Fig. 3(c) can focus the laser beam to subwavelength diameters by the near-field optics effect. Park et al. [23] studied this effect and demonstrated near-field subwavelength focusing of light due to multiple scattering of the light by random nanoparticles in a highly turbid medium. If the scattering process excites the resonant modes of the nanoparticles, redistribution and enhancement of the laser electromagnetic field would occur in a specific region. This effect has been demonstrated in laser surface cleaning [42]. Luk'yanchuk et al. [42] analyzed the scattering of UV radiation at $\lambda_0 = 266$ nm by a SiO_2 particle of radius 0.5 μm using the Mie scattering theory, and showed that the intensity of light at the center of the particle can be up to 60 times higher than that of the incident light due to optical resonance and near-field effects. The nanoparticles of this study, such as Si, Ge, and Ag, may interact with the laser beam through surface plasmon modes [42–45] and the excitation of these modes can be influenced by the droplet temperature. The temperature gradients within the

Optics EXPRESS

microdroplet affect the distribution of the suspended nanoparticles due to convection caused by the variations in the density and surface tension of the liquid in the droplet. The suspended nanoparticles will, therefore, create a random coupling of excited plasmon modes resulting in a more complicated pattern of the laser electromagnetic field that induces randomized deposition of nanodots as in Figs. 4 and 5.

However, the laser-nanoparticle interaction is not applicable to the mechanism for the formation of subwavelength holes when the microdroplets did not carry nanoparticles. The subwavelength focusing, in this case, may be attributed to the variation of temperature by direct laser heating and subsequent convection of the liquid, resulting in a refractive index distribution inside the droplet. High-temperature liquid or vapor bubbles are produced particularly at the focal volume of the laser beam. This hot liquid or bubbles are surrounded by cooler liquid, yielding a core and an outer shell of low and high refractive index regions respectively. The formation of evanescent waves at the core-shell interface when the laser beam travels from the optically denser medium to lighter medium enables subwavelength focusing by the droplets. The curved interface and the variation of refractive index in the denser medium can bend various rays of the laser beam into different angles so that certain bundles of the ray may incident on the core-shell interface at a supercritical angle which is larger than the critical angle for total internal reflection. Under this condition, evanescent waves are generated and these waves decay exponentially with distance into the core but they propagate along the core-shell interface on both sides of the laser incidence point to reach the silicon substrate. These two counter-propagating evanescent waves may interfere to produce a high irradiance spot at the point of contact between the droplet and the substrate. Since the wavelength of evanescent waves is much shorter than that of the incident laser beam, the diameter of the high irradiance interference spot is expected to be much smaller than the focused spot diameter of the original laser beam. By this mechanism, the evanescent waves can produce subwavelength features such as ~100 nm diameter holes in the silicon substrate when the microdroplets do not carry any nanoparticles, as is clear from Fig. 6(a), or ~500 nm nanodots when the microdroplets carry nanoparticles, as shown in Figs. 4(a) and 5(a).

5. Conclusion

This study demonstrates that subwavelength structures can be produced using the interaction between lasers and microdroplets. In this process, the microdroplets are generated from a suspension of nanoparticles using an electrospray technique and they perform the dual roles of carrying nanoparticles and simultaneously acting as superlenses for subwavelength focusing. The superlens characteristics of these microdroplets are attributed to the variation in the refractive index of the droplets when they contain no nanoparticles and to the evanescent waves when the droplets contain nanoparticles. Results show that tiny features can be created by squeezing a laser beam of wavelength λ_0 = 1064 nm into subwavelength regions up to $\lambda_0/10$. While this process is demonstrated to produce subwavelength holes and nanodots, the process is scalable to produce thin films and lines.

Funding

National Science Foundation (1563448).

Acknowledgments

This work was supported by the Manufacturing Machines and Equipment Program in the Division of Civil, Mechanical and Manufacturing Innovation at the Directorate for Engineering in National Science Foundation (1563448). The authors express special thanks to the UCF graduate students, Tianyi Li, Arifur Rahaman and Mohammad Jobayer Hossain, for measuring the reflectance and absorption coefficient. Also the authors appreciate Prof.

Optics EXPRESS

Hyoung Cho's and his post-doctoral research associate Dr. Pawan Pathak's assistance in evaluating the film quality for Fig. 9(b).

Disclosures

"The authors declare that there are no conflicts of interest related to this article."

References

1. T. H. Han, Y. Lee, M. R. Choi, S. H. Woo, S. H. Bae, B. H. Hong, J. H. Ahn, and T. W. Lee, "Extremely efficient flexible organic light-emitting diodes with modified graphene anode," Nat. Photonics **6**(2), 105–110 (2012).
2. B. D. Gates, "Flexible electronics," Science **323**(5921), 1566–1567 (2009).
3. M. Vomero, E. Castagnola, F. Ciarpella, E. Maggiolini, N. Goshi, E. Zucchini, S. Carli, L. Fadiga, S. Kassegne, and D. Ricci, "Highly stable glassy carbon interfaces for long-term neural stimulation and low-noise recording of brain activity," Sci. Rep. **7**(1), 40332 (2017).
4. H. An, T. Habib, S. Shah, H. Gao, M. Radovic, M. J. Green, and J. L. Lutkenhaus, "Surface- agnostic highly stretchable and bendable conductive mxene multilayers," Sci. Adv. **4**, 118 (2018).
5. J. Thomas, P. Gangopadhyay, E. Araci, R. A. Norwood, and N. Peyghambarian, "Nanoimprinting by melt processing: an easy technique to fabricate versatile nanostructures," Adv. Mater. **23**(41), 4782–4787 (2011).
6. T. Y. Liu, H. C. Liao, C. C. Lin, S. H. Hu, and S. Y. Chen, "Biofunctional ZnO nanorod arrays grown on flexible substrates," Langmuir **22**(13), 5804–5809 (2006).
7. A. Nadarajah, R. C. Word, J. Meiss, and R. Könenkamp, "Flexible inorganic nanowire light-emitting diode," Nano Lett. **8**(2), 534–537 (2008).
8. Q. Cao, S. H. Hur, Z. T. Zhu, Y. Sun, C. Wang, M. A. Meitl, M. Shim, and J. A. Rogers, "Highly bendable, transparent thin film transistors that use carbon nanotube based conductors and semiconductors with elastomeric dielectrics," Adv. Mater. **18**(3), 304–309 (2006).
9. Y. M. Li, W. Kim, Y. G. Zhang, M. Rolandi, D. W. Wang, and H. J. Dai, "Growth of single-walled carbon nanotubes from discrete catalytic nanoparticles of various sizes," J. Phys. Chem. B **105**(46), 11424–11431 (2001).
10. B. Y. Ahn, E. B. Duoss, M. J. Motala, X. Guo, S. I. Park, Y. Xiong, J. Yoon, R. G. Nuzzo, J. A. Rogers, and J. A. Lewis, "Omnidirectional printing of flexible, stretchable, and spanning silver microelectrodes," Science **323**(5921), 1590–1593 (2009).
11. H. H. Lee, K. S. Chou, and K. C. Huang, "Inkjet printing of nanosized silver colloids," Nanotechnology **16**(10), 2436–2441 (2005).
12. M. S. Saleh, C. Hu, and R. Panat, "Three-dimensional microarchitected materials and devices using nanoparticle assembly by pointwise spatial printing," Sci. Adv. **3**(3), e1601986 (2017).
13. M. L. Tseng, B. H. Chen, C. H. Chu, C. M. Chang, W. C. Lin, N. N. Chu, M. Mansuripur, A. Q. Liu, and D. P. Tsai, "Fabrication of phase-change chalcogenide Ge2Sb2Te5 patterns by laser-induced forward transfer," Opt. Express **19**(18), 16975–16984 (2011).
14. C. H. Chu, M. L. Tseng, C. Da Shiue, S. W. Chen, H.-P. Chiang, M. Mansuripur, and D. P. Tsai, "Fabrication of phase-change Ge2Sb2Te5 nano-rings," Opt. Express **19**(13), 12652–12657 (2011).
15. A. I. Kuznetsov, J. Koch, and B. N. Chichkov, "Laser-induced backward transfer of gold nanodroplets," Opt. Express **17**(21), 18820–18825 (2009).
16. M. Zheng, M. Yu, Y. Liu, R. Skomski, S. H. Liou, D. J. Sellmyer, V. N. Petryakov, Y. K. Verevkin, N. I. Polushkin, and N. N. Salashchenko, "Magnetic nanodot arrays produced by direct laser interference lithography," Appl. Phys. Lett. **79**(16), 2606–2608 (2001).
17. S. Jeon, V. Malyarchuk, J. A. Rogers, and G. P. Wiederrecht, "Fabricating three-dimensional nanostructures using two photon lithography in a single exposure step," Opt. Express **14**(6), 2300–2308 (2006).
18. Z. C. Chen, N. R. Han, Z. Y. Pan, Y. D. Gong, T. C. Chong, and M. H. Hong, "Tunable resonance enhancement of multi-layer terahertz metamaterials fabricated by parallel laser micro-lens array lithography on flexible substrates," Opt. Mater. Express **1**(2), 151–157 (2011).
19. Z. Wang, M. Hong, B. S. Luk'yanchuk, Y. Lin, Q. F. Wang, and T. C. Chong, "Angle effect in laser nanopatterning with particle-mask," J. Appl. Phys. **96**(11), 6845–6850 (2004).
20. Z. Wang, W. Guo, L. Li, B. Luk'yanchuk, A. Khan, Z. Liu, Z. Chen, and M. Hong, "Optical virtual imaging at 50 nm lateral resolution with a white-light nanoscope," Nat. Commun. **2**(1), 218 (2011).
21. E. Bor, M. Turduev, and H. Kurt, "Differential evolution algorithm based photonic structure design: numerical and experimental verification of subwavelength λ/5 focusing of light," Sci. Rep. **6**(1), 30871 (2016).
22. J. Guan, J. Lin, Y. Ma, J. Tan, and P. Jin, "Subwavelength spot and a three-dimensional optical trap formed by a single planar element with azimuthal light," Sci. Rep. **7**(1), 7380 (2017).
23. J. H. Park, C. Park, H. S. Yu, J. Park, S. Han, J. Shin, S. H. Ko, K. T. Nam, Y. H. Cho, and Y. K. Park, "Subwavelength light focusing using random nanoparticles," Nat. Photonics **7**(6), 454–458 (2013).
24. J. Park, C. Park, K. Lee, Y.-H. Cho, and Y. Park, "Time-reversing a monochromatic subwavelength optical focus by optical phase conjugation of multiply-scattered light," Sci. Rep. **7**(1), 41384 (2017).

Optics EXPRESS

25. H. J. Münzer, M. Mosbacher, M. Bertsch, J. Zimmermann, P. Leiderer, and J. Boneberg, "Local field enhancement effects for nanostructuring of surfaces," J. Microsc. **202**(1), 129–135 (2001).
26. S. Theppakuttai and S. Chen, "Nanoscale surface modification of glass using a 1064 nm pulsed laser," Appl. Phys. Lett. **83**(4), 758–760 (2003).
27. V. N. Smolyaninova, I. I. Smolyaninov, A. V. Kildishev, and V. M. Shalaev, "Maxwell fish-eye and Eaton lenses emulated by microdroplets," Opt. Lett. **35**(20), 3396–3398 (2010).
28. M. Duocastella, C. Florian, P. Serra, and A. Diaspro, "Sub-wavelength laser nanopatterning using droplet lenses," Sci. Rep. **5**(1), 16199 (2015).
29. A. Sobhani, A. Manjavacas, Y. Cao, M. J. McClain, F. J. García de Abajo, P. Nordlander, and N. J. Halas, "Pronounced linewidth narrowing of an aluminum nanoparticle plasmon resonance by interaction with an aluminum metallic film," Nano Lett. **15**(10), 6946–6951 (2015).
30. G. Grinblat, Y. Li, M. P. Nielsen, R. F. Oulton, and S. A. Maier, "Enhanced third harmonic generation in single germanium nanodisks excited at the anapole mode," Nano Lett. **16**(7), 4635–4640 (2016).
31. M. L. Tseng, C. M. Chang, B. H. Cheng, P. C. Wu, K. S. Chung, M. K. Hsiao, H. W. Huang, D. W. Huang, H. P. Chiang, P. T. Leung, and D. P. Tsai, "Multi-level surface enhanced Raman scattering using AgOx thin film," Opt. Express **21**(21), 24460–24467 (2013).
32. A. I. Kuznetsov, A. E. Miroshnichenko, Y. H. Fu, J. Zhang, and B. Luk'yanchuk, "Magnetic light," Sci. Rep. **2**(1), 492 (2012).
33. X. Y. Zhang, A. Hu, T. Zhang, W. Lei, X. J. Xue, Y. Zhou, and W. W. Duley, "Self-assembly of large-scale and ultrathin silver nanoplate films with tunable plasmon resonance properties," ASC nano **5**, 9082–9092 (2011).
34. M. Semmlinger, M. L. Tseng, J. Yang, M. Zhang, C. Zhang, W. Y. Tsai, D. P. Tsai, P. Nordlander, and N. J. Halas, "Vacuum Ultraviolet Light-Generating Metasurface," Nano Lett. **18**(9), 5738–5743 (2018).
35. E. Castillo-Orozco, A. Kar, and R. Kumar, "Electrospray mode transition of microdroplets with semiconductor nanoparticle suspension," Sci. Rep. **7**(1), 5144 (2017).
36. Z. B. Wang, B. S. Luk'yanchuk, M. H. Hong, Y. Lin, and T. C. Chong, "Energy flow around a small particle investigated by classical Mie theory," Phys. Rev. B Condens. Matter Mater. Phys. **70**(3), 035418 (2004).
37. S. Lee, L. Li, Y. Ben-Aryeh, Z. Wang, and W. Guo, "Overcoming the diffraction limit induced by microsphere optical nanoscopy," J. Opt. **15**(12), 125710 (2013).
38. J. C. Burton, A. L. Sharpe, R. C. van der Veen, A. Franco, and S. R. Nagel, "Geometry of the vapor layer under a Leidenfrost drop," Phys. Rev. Lett. **109**(7), 074301 (2012).
39. F. Celestini, T. Frisch, and Y. Pomeau, "Take Off of Small Leidenfrost Droplets," Phys. Rev. Lett. **109**(3), 034501 (2012).
40. J. C. Miñano, "Perfect imaging in a homogeneous threedimensional region," Opt. Express **14**(21), 9627–9635 (2006).
41. J. C. Miñano, P. Benítez, and J. C. González, "Perfect imaging with geodesic waveguides," New J. Phys. **12**(12), 123023 (2010).
42. B. S. Luk'yanchuk, Y. W. Zheng, and Y. Lu, "Laser cleaning of solid surface: optical resonance and near-field effects," High-Power Laser Ablation III **4065**, 576–587 (2000).
43. Y. W. Zheng, B. S. Luk'yanchuk, Y. F. Lu, W. D. Song, and Z. H. Mai, "Dry laser cleaning of particles from solid substrates: experiments and theory," J. Appl. Phys. **90**(5), 2135–2142 (2001).
44. A. I. Kuznetsov, A. E. Miroshnichenko, M. L. Brongersma, Y. S. Kivshar, and B. Luk'yanchuk, "Optically resonant dielectric nanostructures," Science **354**(6314), aag2472 (2016).
45. L. Boris, Zheludev, I. N. Maier, A. Stefan, J. H. Naomi, N. Peter, G. Harald, and C. C. Tow, "The Fano resonance in plasmonic nanostructures and metamaterials," Nat. Mater. **9**, 707 (2010).